Dalton Transactions

PAPER

View Article Online
View Journal | View Issue

Cite this: *Dalton Trans.*, 2014, **43**, 16800

Blue-shift of Eu^{2+} emission in $(Ba,Sr)_3Lu(PO_4)_3:Eu^{2+}$ eulytite solid-solution phosphors resulting from release of neighbouring-cation-induced stress†

Ziyuan Wang,[a] Zhiguo Xia,*[a,b] Maxim S. Molokeev,[c] Victor V. Atuchin[d,e,f] and QuanLin Liu[b]

Received 31st July 2014,
Accepted 11th September 2014

DOI: 10.1039/c4dt02319f

www.rsc.org/dalton

A series of iso-structural eulytite-type $(Ba,Sr)_3Lu(PO_4)_3:Eu^{2+}$ solid-solution phosphors with different Sr/Ba ratios were synthesized by a solid-state reaction. Crystal structures of $(Ba,Sr)_3Lu(PO_4)_3:Eu^{2+}$ were resolved by the Rietveld method, which shows an eulytite-type cubic $Bi_4(SiO_4)_3$ structure with cations disordered in a single C_3 site while the oxygen atoms were distributed over two partially occupied sites. The emission peaks of $Ba_{(3-x)}Sr_xLu(PO_4)_3:Eu^{2+}$ ($0 \le x \le 3$) phosphors were blue-shifted, from 506 to 479 nm, with increasing Sr/Ba ratio upon the same excitation wavelength of 365 nm, and such interesting luminescence behaviours can also be found in other eulytite-type $(Ba,Sr)_3Ln(PO_4)_3:Eu^{2+}$ (Ln = Y, Gd) solid-solution phosphors. The blue-shift of the Eu^{2+} emission with increasing Sr/Ba ratio was ascribed to the variation of the crystal field strength that the 5d orbital of Eu^{2+} ion experiences, and a new model based on the Eu–O bond length and released neighboring-cation stress in disordered $Ba^{2+}/Sr^{2+}/Ln^{3+}$ sites is proposed.

1. Introduction

The cubic structure of the mineral eulytite, $Bi_4(SiO_4)_3$, in the space group $I\bar{4}3d$, was first determined by Menzer.[1] Since then, a great number of eulytite-type compounds have been reported, such as $B^{II}{}_3M^{III}(PO_4)_3$, $B^{II}{}_4(PO_4)_2(SO_4)$, and $B^{II}{}_{7/2}M^{IV}{}_{1/2}(PO_4)_3$, where B^{II} = divalent cation, M^{III} = trivalent cation, M^{IV} = tetravalent cation.[2,3] Among them, cubic $Ba_3La(PO_4)_3$ was first reported by Barbier, where Ba^{2+} and La^{3+} ions were shown to be randomly distributed in one site, and $PO_4{}^{3-}$ tetrahedra found in two different orientations relative to the $(Ba,La)_8$ bisdisphenoid.[2] The current report is about $(Ba,Sr)_3Lu(PO_4)_3:Eu^{2+}$ compounds, which are isostructural to $Ba_3La(PO_4)_3$ with disordered $Ba^{2+}/Sr^{2+}/Lu^{3+}$ sites. Although eulytite-type orthophosphate compounds have been widely reported as hosts for phosphors because of their excellent thermal stability and luminescence properties , there are few studies about their structural properties, and the relationships between crystal structure and Eu^{2+} emission is especially unclear.[4–9] In general, Eu^{2+}-doped phosphors possess a broad-band emission owing to the transition between the 4f ^{6}5d excited-state configuration and the $^8S_{7/2}$ ($4f^7$) ground state. When exposed to the external environment, the 5d energy level is influenced by the surroundings. Thus, enhancement of crystal field strength could lower the 5d ground-state energy level and generate a red shift of the emission peaks.[10] Consequently, a red shift of the Eu^{2+} emission peaks should appear in $(Ba,Sr)_3Lu(PO_4)_3:Eu^{2+}$ with an increasing ratio of Sr/Ba owing to the stronger crystal field of Sr^{2+} as compared with that of Ba^{2+}. However, an unexpected blue-shift of Eu^{2+} emission was observed in this system. Furthermore, after summarizing the Eu^{2+} emission character of the isostructural $M_3Ln(PO_4)_3:Eu^{2+}$ (M = Sr, Ba; Ln = Y, Gd and Lu) compounds in Table 1, we found that blue-shift behaviour is common in such phosphor systems, which should be related to the unusual structural character of the eulytite cubic structure.[4–9] Therefore, it is essential to understand the relationship between the eulytite-type structure and luminescence properties of $(Ba,Sr)_3Lu(PO_4)_3:Eu^{2+}$. The effect of varying the structure on the Eu^{2+} emission and control of the luminescence properties will be of interest for the discovery of new phosphors and the tailoring of their emission behaviours.

[a]*School of Materials Sciences and Technology, China University of Geosciences, Beijing 100083, China*
[b]*School of Materials Sciences and Engineering, University of Science and Technology Beijing, Beijing 100083, China. E-mail: xiazg@ustb.edu.cn; Fax: +86-10-823-77955; Tel: +86-10-823-77955*
[c]*Laboratory of Crystal Physics, Kirensky Institute of Physics, SB RAS, Krasnoyarsk 660036, Russia*
[d]*Laboratory of Optical Materials and Structures, Institute of Semiconductor Physics, SB RAS, Novosibirsk 630090, Russia*
[e]*Functional Electronics Laboratory, Tomsk State University, Tomsk 634050, Russia*
[f]*Laboratory of Semiconductor and Dielectric Materials, Novosibirsk State University, Novosibirsk 630090, Russia*

†Electronic supplementary information (ESI) available: Powder XRD patterns for Rietveld structure analysis, the main parameters of processing and refinement, fractional atomic coordinates, isotropic displacement parameters and main bond lengths for $[Ba_{(3-x)}Sr_{(x)}]_{0.97}Lu(PO_4)_3:0.03Eu^{2+}$ (x = 0, 1, 2 and 3) are shown. CIF files of $[Ba_{(3-x)}Sr_{(x)}]_{0.97}Lu(PO_4)_3:0.03Eu^{2+}$ (x = 0, 1, 2 and 3) are also shown. See DOI: 10.1039/c4dt02319f

Table 1 Eu^{2+} emission in different eulytite-type $B^{II}_3M^{III}(PO_4)_3:Eu^{2+}$ phosphors

Chemical formula	Peak wavelength of Eu^{2+} emission (nm)	Wavelength of blue-shift (nm)	Ref.
$Ba_3Y(PO_4)_3:Eu^{2+}$	556	66	4
$Sr_3Y(PO_4)_3:Eu^{2+}$	490		5
$Ba_3Gd(PO_4)_3:Eu^{2+}$	540	40	6
$Sr_3Gd(PO_4)_3:Eu^{2+}$	500		7
$Ba_3Lu(PO_4)_3:Eu^{2+}$	514/506	25/27	8/This work
$Sr_3Lu(PO_4)_3:Eu^{2+}$	489/479		9/This work

2. Experimental

2.1 Materials and synthesis

$[Ba_{(3-x)}Sr_{(x)}]_{0.97}Lu(PO_4)_3:0.03Eu^{2+}$ ($0 \le x \le 3$) samples were synthesized in the solid state at high temperatures, starting from a mixture containing $BaCO_3$(A.R. 99.9%), $SrCO_3$(A.R. 99.9%), Lu_2O_3(A.R. 99.9%), Eu_2O_3(A.R. 99.9%), and $NH_4H_2(PO_4)_3$(A.R. 99.9%) at the specified stoichiometric ratio. After thorough grinding, the mixtures were placed into an alumina crucible and then sintered at 1300 °C for 4 h under a 10% H_2–90% N_2 gas mixture. Finally the as-synthesized samples were slowly cooled to room temperature.

2.2 Characterization

Powder X-ray diffraction (Bruker AXS D8, 40 kV and 40 mA, Cu-Kα, λ = 0.15405 nm) was used for structural phase identification in the 2θ range from 10° to 120°. Excitation and emission spectra were measured at room temperature using a fluorescence spectrophotometer (F-4600, HITACHI, Japan) with a photomultiplier tube operating at 500 V, and a 150 W Xe lamp used as the excitation lamp. The temperature-dependent luminescence properties were measured on the same spectrophotometer, which was combined with an in-house-constructed heating cell and a computer-controlled electric furnace.

3. Results and discussion

3.1 Phase structure analysis

The XRD patterns of $[Ba_{(3-x)}Sr_{(x)}]_{0.97}Lu(PO_4)_3:0.03Eu^{2+}$ ($0 \le x \le 3$) samples are shown in Fig. 1a. All the diffraction peaks were well indexed to the standard data of $Ba_3Lu(PO_4)_3$ with JCPDS file no. 43-0212, indicating that Eu^{2+} and Sr^{2+} ions could successfully incorporate in the host structure. The characteristic (310) diffraction peak was observed to shift to higher angles with increasing Sr^{2+} content owing to the smaller ionic radius of Sr^{2+} compared with that of Ba^{2+}, as shown in Fig. 1b, further suggesting that continuous solid solutions with different Ba/Sr ratios were formed. Furthermore, Rietveld structural refinements of $[Ba_{(3-x)}Sr_{(x)}]_{0.97}Lu(PO_4)_3:0.03Eu^{2+}$ (x = 0, 1, 2 and 3) were performed using TOPAS 4.2.[11] Initial parameters were obtained from the $Ba_3La(PO_4)_3$ structural model.[2] The detailed powder XRD patterns for Rietveld structure analysis for every composition and the main processing and refinement parameters, including fractional atomic coordinates, isotropic displacement parameters and main bond lengths are shown, respectively, in Fig. S1–S4 and Tables S1–S3, in ESI.† The refinements confirmed the eulytite-type single-phased nature of $[Ba_{(3-x)}Sr_{(x)}]_{0.97}Lu(PO_4)_3:0.03Eu^{2+}$ (x = 0, 1, 2 and 3). The related CIF files for the four compositions of $[Ba_{(3-x)}Sr_{(x)}]_{0.97}Lu(PO_4)_3:0.03Eu^{2+}$ (x = 0, 1, 2 and 3) can be found in the ESI† materials.

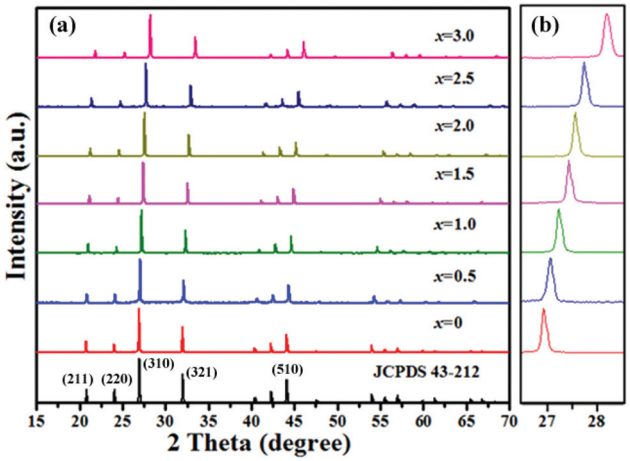

Fig. 1 (a) XRD patterns of the $Ba_{3-x}Sr_xLu(PO_4)_3:Eu^{2+}$($0 \le x \le 3$) samples, and (b) a magnified view of the (310) diffraction peak as a function of x.

A representative structure of $Ba_{3-x}Sr_xLu(PO_4)_3:Eu^{2+}$, in space group $I\bar{4}3d$, is shown in Fig. 2a. In this structure, the $Ba^{2+}/Sr^{2+}/Lu^{3+}/Eu^{2+}$ cations are randomly distributed in a single site. Meanwhile, the $(Ba,Sr)_3Lu(PO_4)_3$ host was observed to possess two different orientations of the $[PO_4]^{3-}$ tetrahedrons within the $(Sr,Ba,Lu)_8$ bisdisphenoid corresponding to two sets of partially occupied oxygen positions O1 and O2, as shown in Fig. 2a. Accordingly, the $(Ba,Sr)_3Lu(PO_4)_3$ phase showed not only the cation disorder but also an oxygen sublattice disorder.[2,7] Although Eu^{2+} ions were expected to be the primary ions to substitute for Ba^{2+} and Sr^{2+} due to the same valence, Eu^{2+}, Ba^{2+}, Sr^{2+}, and Lu^{3+} ions were all found to be occupying a single C_3 site. Fig. 2b shows the coordination environment of Ba^{2+}, Sr^{2+}, Lu^{3+}, and Eu^{2+} in C_3 sites. These C_3 sites were randomly occupied by the four ions, which showed a coordination number of 12, with 6 short-range (2.3–2.5 Å) and 6 long-range (2.6–2.97 Å) oxide bonds as shown in Fig. 2b; these two sets of bonds correspond to the two disordered oxygen atoms O1 and O2 in the lattice. Unfortunately, X-ray diffraction gives only average bond lengths d(Ba/Sr/Lu/Eu–O) and it is impossible to determine the value of each bond length from the d(Ba–O), d(Sr–O), d(Lu–O) and d(Eu–O) set. However, the details of their variations will be discussed below. The cell volume V varies directly with x, as is clearly evident in Fig. 2c, which shows that the nominal chemical formula $Ba_{3-x}Sr_xLu(PO_4)_3:Eu^{2+}$ ($0 \le x \le 3$) is close to the real chemical formula at least with respect to Ba/Sr ratios, and Ba/Sr substitution excellently obeys Vegard's rule for structural parameters.

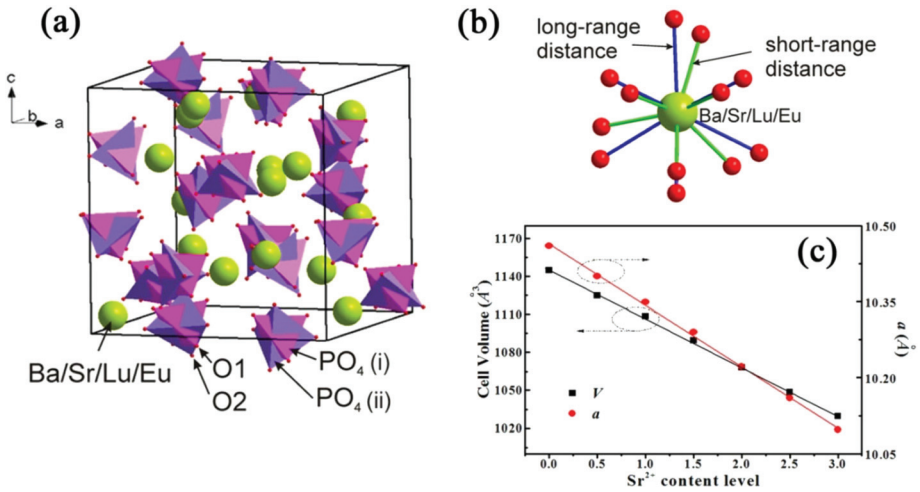

Fig. 2 (a) Crystal structure of $Ba_3Sr_{3-x}Lu(PO_4)_3:Eu^{2+}$ ($0 \le x \le 3$); (b) coordination environment of Ba/Sr/Lu/Eu cations; (c) dependence of lattice parameters *V* and *a* on Sr^{2+} content.

3.2 Analysis of photoluminescence properties

Fig. 3a shows the photoluminescence emission (PL) and photoluminescence excitation (PLE) spectra obtained from $[Ba_{(3-x)}Sr_{(x)}]_{0.97}Lu(PO_4)_3:0.03Eu^{2+}$ ($0 \le x \le 3$) samples. All the PLE spectra exhibit a broad excitation band from 240 to 420 nm originating from the f–d transition of Eu^{2+} ions, as given in the inset of Fig. 3a. The normalized PL spectra also show the broadband emission, and the peak wavelengths are blue-shifted from 503 to 471 nm with increasing Sr^{2+} content. From Fig. 3b it is also clearly seen that both the full width half maximum values (FWHM) and emission peak wavelengths of $Ba_{(3-x)}Sr_xLu(PO_4)_3:0.03Eu^{2+}$ decrease as *x* increases, indicating that the emission centres experienced a weaker crystal field strength. Fig. 3c shows the temperature dependence of emission intensities of $Ba_{(3-x)}Sr_xLu(PO_4)_3:0.03Eu^{2+}$($x$ = 0, 1, 2, 3) phosphors, recorded between 30 °C and 150 °C. The emission intensities for the studied phosphor samples were observed to decrease with increasing temperature due to the thermal quenching effect.[12] However, it was also clearly found that the thermal stability is enhanced with the incorporation of Sr^{2+} in the host. Furthermore, Fig. 3d shows that, in the four samples of the $Ba_{(3-x)}Sr_xLu(PO_4)_3:0.03Eu^{2+}$ (x = 0, 1, 2, 3) series, all the FWHMs decrease and the emission peaks shift to short wavelengths (blue-shift) with increasing temperature. The decrease in FWHMs and the temperature-induced blue-shift in the respective samples indicate that thermally active phonon-assisted tunneling from the excited states of the low-energy emission band to the excited states of the high-energy emission band occurred.[13]

3.3 Proposed mechanism for the blue-shifted Eu^{2+} emission

As mentioned above, a red shift of the Eu^{2+} emission would be expected to occur in $(Ba,Sr)_3Lu(PO_4)_3:Eu^{2+}$ with increasing Sr/Ba ratio based on the stronger crystal field of Sr^{2+} as compared with that of Ba^{2+}. However, the observed blue-shifted Eu^{2+} emission in this system may be related to the rigid eulytite cubic structure and the cation's sites having been occupied by several types of ions with correspondingly varying bond lengths. Therefore, a schematic diagram of the average Ba/Sr/Lu/Eu–O bond length in $Ba_{3-x}Sr_xLu(PO_4)_3:Eu^{2+}$ is presented in Fig. 4a. As mentioned previously, $Eu^{2+}/Ba^{2+}/Sr^{2+}/Lu^{3+}$ ions should be disordered in a single C_3 site. From our structural model and refinement results, which show disorder of the $Ba^{2+}/Sr^{2+}/Lu^{3+}/Eu^{2+}$ ions, it is impossible for us to find exact bond lengths of *d*(Ba–O), *d*(Sr–O), *d*(Lu–O) and *d*(Eu–O) individually, and only average bond lengths of *d*(Ba/Sr/Lu/Eu–O) can be revealed (Table S3†). Two types of Ba/Sr/Lu/Eu–O bonding can be found in the coordination of $Ba^{2+}/Sr^{2+}/Lu^{3+}/Eu^{2+}$ ions. One belongs to the short-range bonds (2.3–2.5 Å) and the other is long-range ones (2.6–2.97 Å). In Fig. 4b, one can see that the short-range bond lengths first increase and then decrease as *x* increases (line 2) whereas the long-range ones decrease (line 1). Meanwhile, the average of all bond lengths *d*(Ba/Sr/Lu/Eu–O) decreases as *x* increases (line 3) in accordance with the cell volume decrease. This proves that some stretching of the bonds occurs in the crystals with increasing Sr^{2+} content and indicates why the emission peaks shift to the shorter wavelength region with incorporation of Sr^{2+} ions. However, the variation of *d*(Eu–O) is indirectly related to the observed blue-shifting of Eu^{2+} through the variation of the crystal field strength impacts on the external orbitals of Eu^{2+} ions. Calculations of these crystal field strengths by first-principles methods may be carried out during future work.[14]

A model of structural changes with varying Sr^{2+} content is proposed herein to account for the blue-shift behaviour of the emission spectra, and is shown in Fig. 4c. Since $Eu^{2+}/Ba^{2+}/Sr^{2+}/Lu^{3+}$ ions were disordered in a single C_3 site, Eu–O bond lengths could be greatly influenced by surrounding ions. According to this model, in the (Sr^{2+}-free) Ba_3Lu-

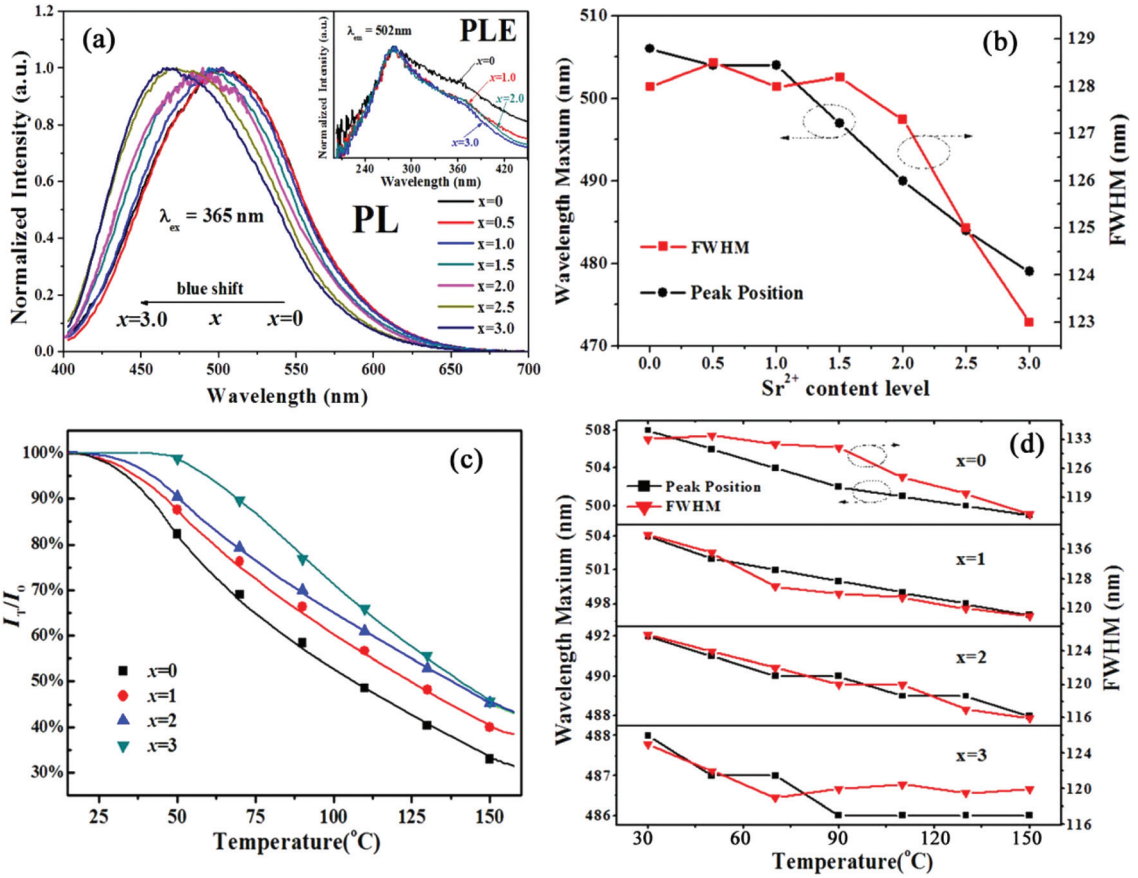

Fig. 3 (a) PL and PLE spectra of $[Ba_{(3-x)}Sr_{(x)}]_{0.97}Lu(PO_4)_3{:}0.03Eu^{2+}$ ($0 \le x \le 3$); (b) dependence of the FWHM and the peak positions on Sr^{2+} content; (c) dependence of the peak emission intensity of $Ba_{(3-x)}Sr_xLu(PO_4)_3{:}0.03Eu^{2+}$ (x = 0, 1, 2, 3) on temperature; (d) the temperature dependence of the FWHMs and the peak positions for each composition.

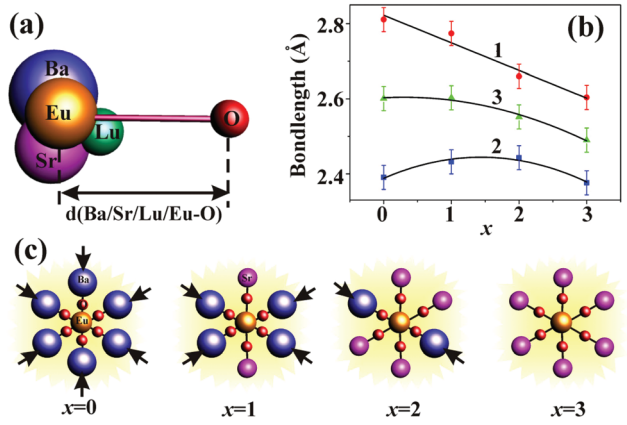

Fig. 4 (a) Schematic diagram of the average Ba/Sr/Lu/Eu–O bond length in $[Ba_{(3-x)}Sr_{(x)}]_{0.97}Lu(PO_4)_3{:}0.03Eu^{2+}$; (b) average bond lengths at different values of x: (1) long-range bonds; (2) short-range bonds; (3) both short- and long-range bonds in crystals; (c) schematic figures showing the Eu–O environment and neighbouring-cation effect in $[Ba_{(3-x)}Sr_{(x)}]_{0.97}Lu(PO_4)_3{:}0.03Eu^{2+}$. Arrows indicate compression of Eu–O bonds resulting from Ba^{2+}.

$(PO_4)_3{:}0.03Eu^{2+}$ compound, the large radii of Ba^{2+} ions lead to stressful compression of neighbouring d(Eu–O) bonds, as shown in Fig. 4(c, x = 0). As Sr^{2+} content (*i.e.*, x) increases in $Ba_{(3-x)}Sr_xLu(PO_4)_3{:}Eu^{2+}$, some stress would be released and diminished owing to the lower ionic radius (IR) of Sr^{2+} (at 1.18 Å) than of Ba^{2+} (at 1.35 Å), and the bond length of d(Eu–O) would increase (Fig. 4(c, x = 1 and 2)).[15] The crystal field splitting of Eu^{2+} would in turn weaken according to this model, and emission peaks would become blue-shifted. Finally, in (Ba^{2+}-free) $Sr_3Lu(PO_4)_3{:}0.03Eu^{2+}$, the stress would became minimal as the maximal bond length of d(Eu–O) is attained, resulting in a shift of the emission peak to a lowest value. This model can well explain the blue-shift in compounds $(Ba,Sr)_3Lu(PO_4)_3{:}Eu^{2+}$ to a certain extent. In spite of the increase in the bond length of d(Eu–O), the average bond length of d(Ba/Sr/Lu/Eu–O) decreases in $Ba_{3-x}Sr_xLu(PO_4)_3{:}Eu^{2+}$ phosphors with increasing Sr^{2+} content. This is because the contribution of d(Ba–O) to the average bond length lessens with increasing Sr^{2+}, as seen in Fig. 4(c,1–2) while the contribution of d(Eu–O) to the average bond length is very small. So the average bond length d(Ba/Sr/Lu/Eu–O) decreases along with decreasing cell volume and increasing Sr^{2+} content, as shown in Fig. 2c. Moreover, there also exists a local process that increases the d(Eu–O) bond lengths in the crystal. This result shows that the effect of neighbouring cations on the spectroscopic properties of activators is reasonable. Therefore, by such a structural strategy, we can tune and tailor the emis-

sion properties of complex solid-solution phosphors using controlled substitution of different cations in the single sites.[16]

4. Conclusions

In summary, we have synthesized isostructural single-phased $Ba_{(3-x)}Sr_xLu(PO_4)_3:Eu^{2+}$ ($0 \le x \le 3$) phosphors. By gradual substitution of Ba^{2+} with Sr^{2+}, a regular transmutation of cell parameters was found among the XRD patterns. The crystal structure of $(Ba,Sr)Lu(PO_4)_3:Eu^{2+}$ was determined using Rietveld refinement, which shows an eulytite-type structure with cations disordered in a single C_3 site of the $I\bar{4}3d$ space group while the oxygen atoms were distributed over two partially occupied sites. The emission peaks of $Ba_{(3-x)}Sr_xLu(PO_4)_3:Eu^{2+}$ ($0 \le x \le 3$) phosphors were blue-shifted. It is proposed that the d(Eu–O) bond lengths increased as a result of lower stress from smaller Sr^{2+} ions when Sr^{2+} ions replaced Ba^{2+} ions. That results in weakening the Eu^{2+} crystal field splitting from the neighbouring-cation effect, generating the blue-shifts. Thus, tailoring the emission properties of complex solid-solution phosphors can be realized using the controlled substitution of different cations in the single sites, which can be useful for creating new phosphor systems.

Acknowledgements

The present work was supported by the National Natural Science Foundations of China (grant no. 51002146, no. 51272242), Natural Science Foundations of Beijing (2132050), the Program for New Century Excellent Talents in the University of the Ministry of Education of China (NCET-12-0950), Beijing Nova Program (Z131103000413047), Beijing Youth Excellent Talent Program (YETP0635) and the Funds of the State Key Laboratory of New Ceramics and Fine Processing, Tsinghua University (KF201306). V.V.A. is partly supported by the Ministry of Education and Science of the Russian Federation.

References

1 G. Menzer, *Z. Kristallogr.*, 1931, **78**, 136.
2 J. Barbier, *J. Solid State Chem.*, 1992, **101**, 249.
3 G. Blasse, *J. Solid State Chem.*, 1970, **2**, 27.
4 Z. P. Yang, P. F. Liu, J. J. Lia, F. C. Lu and L. Lv, *J. Alloys Compd.*, 2013, **578**, 118.
5 N. Guo, Y. J. Huang, M. Yang, Y. H. Song, Y. H. Zheng and H. P. You, *Phys. Chem. Chem. Phys.*, 2011, **13**, 15077.
6 N. Guo, W. Lü, Y. C. Jia, W. Z. Lv, Q. Zhao and H. P. You, *ChemPhysChem*, 2013, **14**, 192.
7 N. Guo, Y. H. Zheng, Y. C. Jia, H. Qiao and H. P. You, *New J. Chem.*, 2012, **36**, 168.
8 N. Guo, Y. J. Huang, Y. C. Jia, W. Z. Lv, Q. Zhao, W. Lü, Z. G. Xia and H. P. You, *Dalton Trans.*, 2013, **42**, 941.
9 N. Guo, Y. H. Zheng, Y. C. Jia, H. Qiao and H. P. You, *J. Phys. Chem. C*, 2012, **116**, 1329.
10 Z. G. Xia, Y. Y. Zhang, M. S. Molokeev, V. V. Atuchin and Y. Luo, *Sci. Rep.*, 2013, **3**, 3310.
11 *Bruker AXS TOPAS V4: General profile and structure analysis software for powder diffraction data. – User's Manual*. Bruker AXS, Karlsruhe, Germany, 2008.
12 J. S. Kim, Y. H. Park, S. M. Kim, J. C. Choi and H. L. Park, *Solid State Commun.*, 2005, **133**, 445.
13 S. Shionoya and W. M. Yen, *Phosphor Handbook*, CRC Press, New York, 1998.
14 M. G. Brik, *J. Phys. Chem. Solids*, 2007, **68**, 1341.
15 R. D. Shannon, *Acta Crystallogr., Sect. A: Cryst. Phys., Diffr., Theor. Gen. Cryst.*, 1976, **32**, 751.
16 W. Lv, Y. C. Jia, Q. Zhao, W. Z. Lv and H. P. You, *Chem. Commun.*, 2014, **50**, 2635.